Biophysical Journal, Volume *110*

Supplemental Information

Motor Protein Accumulation on Antiparallel Microtubule Overlaps

Hui-Shun Kuan and Meredith D. Betterton

Supporting Material

H.-S. Kuan and M. D. Betterton
(Dated: April 27, 2016)

I. KINETIC MONTE CARLO SIMULATIONS

We performed kinetic Monte Carlo (kMC) simulations of the discrete model with time step Δt and the following rules at each time step for an overlap with $2N$ sites:

1. Randomly choose a filament (R/L) and site i.

2. If the site is empty, attach a motor with probability $k_{\text{on}}c\Delta t$. If the site is occupied, detach the motor with probability $k_{\text{off}}\Delta t$.

3. If the site is occupied and the adjacent site toward the MT plus end is empty, move the motor forward with probability $v\Delta t$.

4. If the site is occupied and the corresponding site on the neighboring MT is empty, switch the motor to the other filament with probability $s\Delta t$.

5. Enforce the boundary conditions: site 1 on filament R and site N on filament L are occupied with probability α, while site N on filament R and site 1 on filament L are occupied with probability $(1-\beta)$.

6. Repeat steps 1-5 $2N$ times total to sample all sites on both MTs.

We typically choose $\Delta t = 5 \times 10^{-4}$ s such that the characteristic time for motor binding/unbinding is about 10^5 time steps, if the bulk motor concentration is 200 nM. To reach steady state we run for 4×10^7 time steps, and then collect data in a measurement run of 2×10^7 time steps. The average motor concentration is obtained by averaging 10^4-10^5 samples, separated by 200 time steps. For simulations of the large-S parameter set, we choose $\Delta t = 5 \times 10^{-6}$ s such that the characteristic time for motor binding/unbinding is about 10^7 steps if the bulk motor concentration is 200 nM.

A. Simulated images

The simulated images of motor density profiles shown in fig. 1B in the main text were created by running kMC simulations with 100 nM bulk motor concentration on a 120-site overlap (0.96 μm long), 25 nM bulk motor concentration on a 360-site overlap (2.88 μm long), and 5 nM bulk motor concentration on a 600-site overlap (4.8 μm long). After the simulation reached steady state, we created the images by sampling the motor density. In the green channel, we approximated a 100-ms experimental exposure by summing instantaneous density profiles from 20 consecutive 0.005 s simulation snapshots. Each motor simulated image produced a Gaussian intensity profile with a standard deviation of 150 nM. The intensity profiles were binned into 150-nm wide simulated pixels. We then added a constant background intensity level and Gaussian noise to each pixel. In the red channel, the overlap was defined by a Gaussian line of constant intensity, with background and noise added. The green and red simulated channels were offset by 2 pixels to simulate chromatic

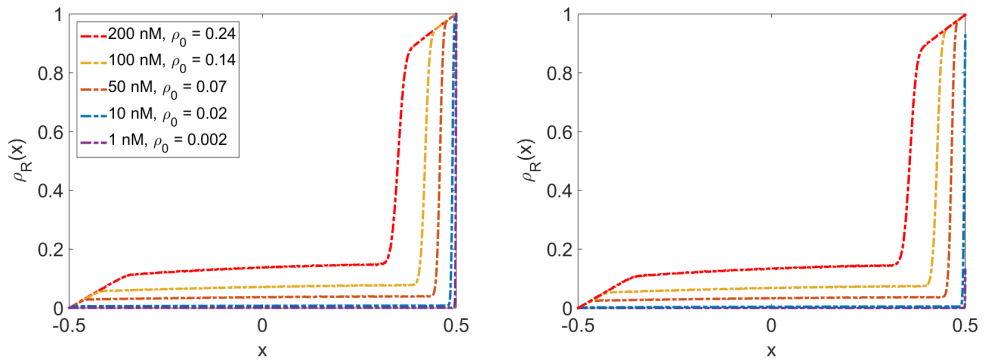

FIG. S1. Comparison of motor density profiles for zero and small β. Left: motor density $\rho_R(x)$ for $\beta = 0$. Right: motor density $\rho_R(x)$ for $\beta = 2.7 \times 10^{-3}$. Other parameters are the reference parameters with motor concentrations as shown in the legend.

aberration. In the blue channel, only background and Gaussian noise were present. The images from each motor concentration were brightness and contrast adjusted.

The simulated motor kymographs shown in fig. 1C in the main text were made by sampling a kMC simulation performed at 0.5 nM bulk motor concentration on a 2500-site overlap (20 μm long). The motor density was sampled every 0.025 s over a 50 s simulation, and the kymograph was constructed from the central 2000 sites of the overlap. Each motor in the simulated kymograph produced a Gaussian intensity profile with a standard deviation of 150 nM. The intensity profiles were binned into 150-nm wide simulated pixels. We then added a constant background intensity level and Gaussian pixel noise. The kymograph was brightness and contrast adjusted.

B. Comparison of zero and small β

In fig. S1 we show simulation results for the reference parameter set for filament flux plus-end boundary conditions with $\beta = 0$ and $\beta = 2.7 \times 10^{-3}$. The density profiles are nearly identical.

II. MEAN-FIELD CONTINUUM MODEL

To derive the mean-field continuum model, we first take the stationary average $\langle \hat{n}_i \rangle \equiv \rho_i$, apply the random phase approximation, $\langle \hat{n}_i \hat{n}_{i+1} \rangle = \langle \hat{n}_i \rangle \langle \hat{n}_{i+1} \rangle$, and assume motor commutation during track switching $\langle \hat{n}_{R,i} \hat{n}_{L,i} \rangle = \langle \hat{n}_{L,i} \rangle \langle \hat{n}_{R,i} \rangle$. The resulting discrete equations in the bulk are

$$\frac{\partial \rho_{R,i}}{\partial t} = -v\rho_{R,i}(1-\rho_{R,i+1}) + v\rho_{R,i-1}(1-\rho_{R,i}) + k_{\text{on}}c(1-\rho_{R,i}) - k_{\text{off}}\rho_{R,i} - s\rho_{R,i} + s\rho_{L,i} \quad \text{(S1)}$$

$$\frac{\partial \rho_{L,i}}{\partial t} = -v\rho_{L,i}(1-\rho_{L,i-1}) + v\rho_{L,i+1}(1-\rho_{L,i}) + k_{\text{on}}c(1-\rho_{L,i}) - k_{\text{off}}\rho_{L,i} - s\rho_{L,i} + s\rho_{R,i} \quad \text{(S2)}$$

and for the boundaries:

$$\frac{\partial \rho_{R,1}}{\partial t} = v\alpha(1-\rho_{R,1}) - v\rho_{R,1}(1-\rho_{R,2}), \quad \text{(S3)}$$

$$\frac{\partial \rho_{R,N}}{\partial t} = -v\beta\rho_{R,N} + v\rho_{R,N-1}(1-\rho_{R,N}), \quad \text{(S4)}$$

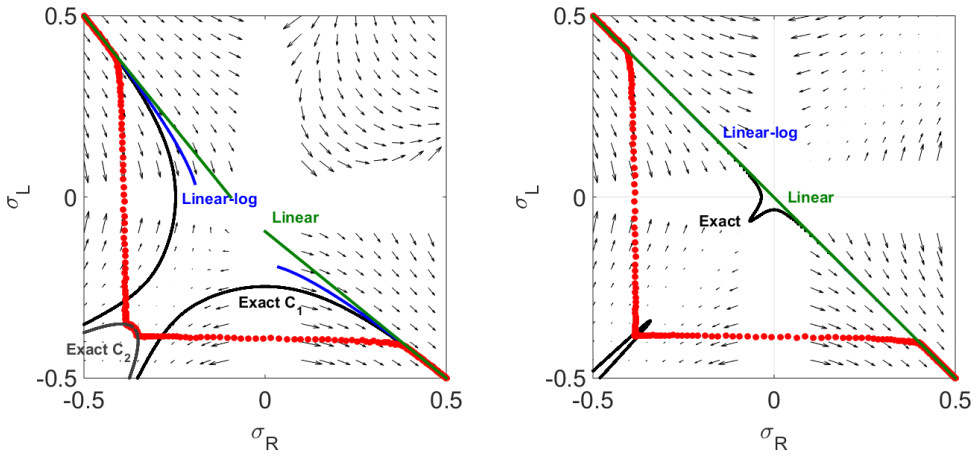

FIG. S2. Phase portraits in the σ_R-σ_L plane. Left: experimental parameter set; right: large-S parameter set. Both use a bulk motor concentration of 200 nM. The arrows indicate the direction of change of the densities as determined by Eqns. S9, S10. Black lines are the exact solutions to the continuum equations (Eqn. S18), red dots are simulation results, green line is the linear approximate solution near the ends of the overlap (Eqns. S19, S20), and blue line is the linear-log approximate solution near the ends of the overlap (Eqns. S23, S24).

and similarly for L.

We take the continuum limit where ρ_i becomes a continuous field $\rho(x)$, and define $\rho_{i\pm1} \to \rho(x \pm \delta)$, where δ is a length per motor binding site on the MT. We Taylor expand $\rho(x \pm \delta)$ to second order and nondimensionalize the parameters and variables by choosing the length of the MT, L, as the unit of length and L/v as the unit of time. We use capital letters to denote the nondimensionalized parameters ($S = sL/v$ and so on). Then the equations become

$$\frac{\partial \rho_R}{\partial t} = \frac{\delta}{2}\frac{\partial^2 \rho_R}{\partial x^2} + (2\rho_R - 1)\frac{\partial \rho_R}{\partial x} + K_{\text{on}}c(1-\rho_R) - K_{\text{off}}\rho_R - S\rho_R + S\rho_L \tag{S5}$$

$$\frac{\partial \rho_L}{\partial t} = \frac{\delta}{2}\frac{\partial^2 \rho_L}{\partial x^2} + (1 - 2\rho_L)\frac{\partial \rho_L}{\partial x} + K_{\text{on}}c(1-\rho_L) - K_{\text{off}}\rho_L + S\rho_R - S\rho_L. \tag{S6}$$

We choose $x = 0$ as the center of the overlap, so the boundary conditions become $\rho_R(-0.5) = \rho_L(0.5) = \alpha$ and $\rho_R(0.5) = \rho_L(-0.5) = 1 - \beta$.

Because δ is small, we typically neglect the second derivative terms. However, if the first derivative terms are close to 0, which occurs when $\rho \approx 1/2$, the second-derivative terms may be important. The steady-state equations with second-derivative terms neglected are

$$0 = (2\rho_R - 1)\frac{\partial \rho_R}{\partial x} + K_{\text{on}}c(1-\rho_R) - K_{\text{off}}\rho_R - S\rho_R + S\rho_L, \tag{S7}$$

$$0 = (1 - 2\rho_L)\frac{\partial \rho_L}{\partial x} + K_{\text{on}}c(1-\rho_L) - K_{\text{off}}\rho_L + S\rho_R - S\rho_L. \tag{S8}$$

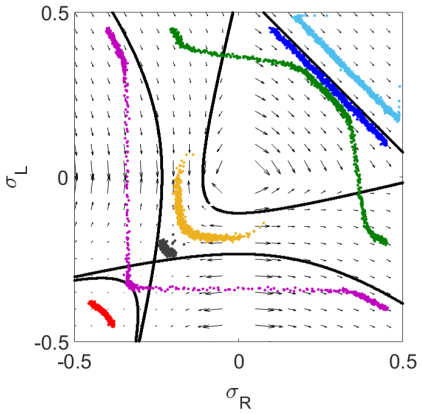

FIG. S3. The phase space flows for the simulations shown in figure 2 in the main text. The parameters used are the reference parameter set of table 1 with a bulk motor concentration of 200 nM, except for the switching rate which is 0.1 s^{-1} and the boundary conditions as noted below. H_n: high-density center-minimum phase ($\alpha = 0.95$, $\beta = 0.99$, light blue). H_x: high-density center-maximum phase ($\alpha = 0.6$, $\beta = 0.95$, dark blue). LH_x: low density-high density center-maximum coexistence ($\alpha = 0.3$, $\beta = 0.95$, green). M: Meissner phase $\alpha = 0.6$, $\beta = 0.4$, yellow). L_n: low-density center-minimum phase ($\alpha = 0.3$, $\beta = 0.4$, black). LH_n: low density-high density center-minimum coexistence ($\alpha = 0.1$, $\beta = 0.95$, magenta). L_x: low-density center-maximum phase ($\alpha = 0.05$, $\beta = 0.1$, red).

A. Exact solution

To find spatially varying solutions to Eqn. S7, S8, we first define $\sigma_{R,L} = \rho_{R,L} - \frac{1}{2}$ as the difference of the densities from 1/2. We also define a shorthand for the rate combinations $k = K_{on}c + K_{off} + S$ and $\gamma = K_{on}c - K_{off}$. Then the equations become

$$\frac{d\sigma_R}{dx} = \frac{k}{2} - \frac{\gamma}{4\sigma_R} - \frac{S\sigma_L}{2\sigma_R} \tag{S9}$$

$$\frac{d\sigma_L}{dx} = -\frac{k}{2} + \frac{\gamma}{4\sigma_L} + \frac{S\sigma_R}{2\sigma_L}. \tag{S10}$$

Eqns S9 and S10 are well defined for $\sigma_{R,L} \neq 0$. Next we introduce the sum and difference of the densities, the total motor concentration $\phi(x) = \sigma_R + \sigma_L$ and $\omega(x) = \sigma_R - \sigma_L$. The equations are

$$\frac{d\phi}{dx} = \frac{\gamma\omega + 2S\phi\omega}{\phi^2 - \omega^2}, \tag{S11}$$

$$\frac{d\omega}{dx} = \frac{(k-S)\phi^2 - \gamma\phi - (k+S)\omega^2}{\phi^2 - \omega^2}, \tag{S12}$$

which can be combined to give

$$\omega\frac{d\omega}{d\phi} = \frac{(k-S)\phi^2 - \gamma\phi - (k+S)\omega^2}{\gamma + 2S\phi}. \tag{S13}$$

Defining $\eta(\phi) = \omega^2(\phi)$, this can be rewritten

$$\frac{1}{2}\frac{d\eta}{d\phi} = \frac{(k-S)\phi^2 - \gamma\phi - (k+S)\eta}{\gamma + 2S\phi}, \tag{S14}$$

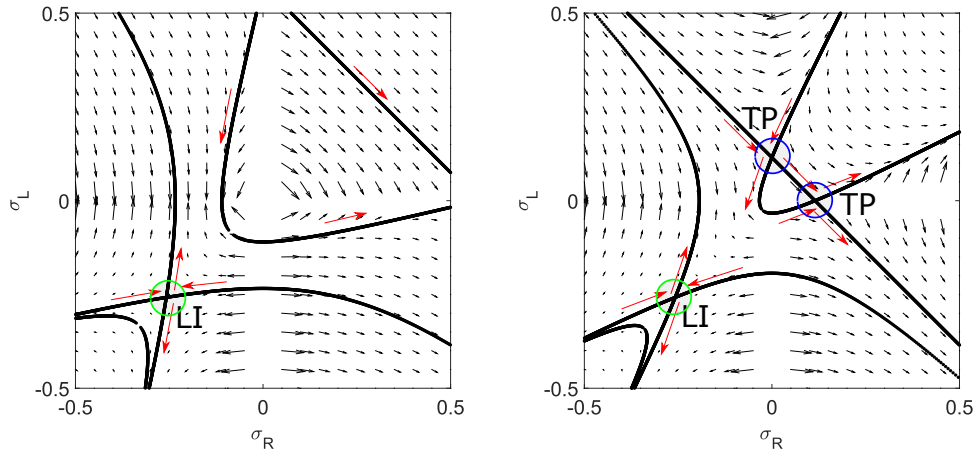

FIG. S4. Phase space flows. Left: low switching rate (0.1 s^{-1}); right, high switching rate (5 s^{-1}). Other parameters are the reference parameter set of table 1 with a bulk motor concentration of 200 nM, except the motor speed is 5 μm s^{-1}. The Langmuir isotherm is labeled LI, and the transition points are labeled TP.

or

$$\frac{\gamma + 2S\phi}{2} d\eta + [\gamma\phi - (k - S)\phi^2 + (k + S)\eta] d\phi = 0. \tag{S15}$$

This inexact ODE can be made exact through multiplication by the integrating factor $(\gamma+2S\phi)^{k/S}$. We then obtain the solution by direct integration,

$$C_1 = \int d\eta \; (\gamma + 2S\phi)^{k/S} \left[\frac{\gamma + 2S\phi}{2}\right] + \int d\phi \; (\gamma + 2S\phi)^{k/S} \left[\gamma\phi - (k - S)\phi^2 + (k + S)\eta\right], \tag{S16}$$

$$C_1 = \frac{\eta}{2}(\gamma + 2S\phi)^{1+k/S} - (\gamma + 2S\phi)^{1+k/S} \frac{\gamma^2 - 2(k + S)\gamma\phi + (k - S)(k + 2S)\phi^2}{2(k + 2S)(k + 3S)}, \tag{S17}$$

which gives the exact solution

$$\omega^2(\phi) = \frac{C}{(\gamma + 2S\phi)^{1+k/S}} - \frac{2(k + S)\gamma\phi - (k - S)(k + 2S)\phi^2 - \gamma^2}{(k + 2S)(k + 3S)}. \tag{S18}$$

Here C_1 and C denote integration constants.

This solution is the relationship between ω and ϕ that satisfies the steady-state equation. This is plotted as the black curves in the phase portraits of figs. S2 – S5. Note that for boundary conditions $\alpha = \beta = 0$, $\sigma_R(\mp 0.5) = \mp 0.5$ and $\sigma_L(\mp 0.5) = \pm 0.5$. Therefore, the filament ends correspond to the upper left and lower right corners in the phase portraits of fig. S2. Other boundary conditions correspond to other pointes in the phase plane. As expected, the direction of change of the exact solutions follow the phase arrows. In fig. S2, the linear and linear-log curves are approximations that hold near the overlap ends, as described below.

We overlaid the results of kMC simulations of the discrete model in red. From this representation, we can see how the phase-plane motor density is connected to the approximately linear variation of motor density: the boundary layers where the motor density is linearly increasing/decreasing show up as the sloped red lines near the upper left and lower right corners of the phase plane. The

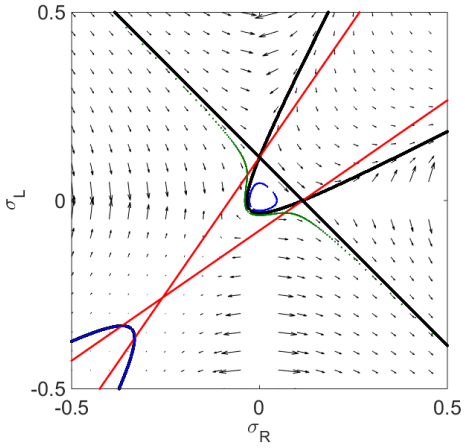

FIG. S5. Phase space flows showing curves adjacent to the the $C = 0$ curve. The green curve has C slightly greater than zero and is an open curve. The blue curve has C slightly less than zero and is a closed curve. The red lines are nullclines.

approximately constant density region in the center of the filaments corresponds to the set of points in the lower left of the phase plane, and the crossover between the boundary layers and the approximately constant region are the red horizontal and vertical lines.

Our simulation results (red) deviate substantially from the exact solutions to the continuum equations (black). In particular, near the overlap edges, the densities follow an exact solution with integration constant C_1, then cross over to an exact solution with integration constant C_2 for the overlap central region. This occurs because the exact solution we found to the continuum equations (Eqn. S18) does not satisfy the nonlocal total binding constraint (Eqn. 11).

III. PHASE DIAGRAM

Similar to the single-filament case [5], we find low density (L), high density (H), low density-high density (LH), and Meissner (M) phases. Low density is < 0.5, and high density > 0.5. Switching between the two antiparallel filaments causes the motor density to become either higher or lower at the center. In addition, for high switching rate a low density-high density-low density-high density (LHLH) phase appears. We describe the conditions for each phase to occur below assuming a rightward-oriented (R) filament, as in fig. 2 in the main text.

The motor density profile is determined by the phase space flow (fig. S3, S4). For low switching rate (fig. S4, left), there is only one fixed point, the Langmuir isotherm. However, once the switching rate becomes sufficiently high, a pair of transition points (TP) appear (fig. S4, right). The transition points are the intersections of the nullclines and the $\sigma = 0$ lines. We call the line which connects the two TP the transition line.

For a fixed overlap length, the total number of lattice sites is constant. Therefore the density profile must connect the starting and ending points with a number of steps equal to the number of sites. If this is not possible, one or both boundary conditions cannot be satisfied.

Symbol	Parameter	Large-S value	Notes
v	Motor speed	0.5 μm s^{-1}	Same as reference parameters
k_{on}	Binding rate constant	2.7×10^{-6} nM^{-1} s^{-1}	Reduced by 10^2 for large-S parameters
c	Bulk motor concentration	1–200 nM	Same as reference parameters
k_{off}	Unbinding frequency	1.69×10^{-3} s^{-1}	Reduced by 10^2 for large-S parameters
s	Switching rate	0.44 s^{-1}	Same as reference parameters
α	Motor flux constant into overlap from MT minus end	0	Same as reference parameters
β	Motor unbinding rate constant from MT plus end	0	Same as reference parameters
N	Number of sites	120-2500	Same as reference parameters
δ	Length of a single site	8 nm	Same as reference parameters

TABLE S1. Model parameters for large-S parameter set. We reduced the binding and unbinding rates by a factor of 10^2 relative to the reference parameters (table 1 in the main text).

1. Low density

The low-density phase occurs when $\alpha < 0.5$ and the right boundary condition cannot be satisfied. If $\alpha < \rho_0$, the motor density profile has a local maximum at the center. If $\alpha > \rho_0$, the motor density profile has a local minimum at the center.

2. Low density-high density

The domain wall occurs where the density changes from L to H. This means the profile crosses the $\sigma = 0$ ($\rho = 1/2$) line. The matching condition between L and H phases is continuity in the current [5] $\rho(x_l) = 1 - \rho(x_r)$ or $\sigma(x_l) = -\sigma(x_r)$. We determine the domain wall position using the symmetry of the total motor density in the overlap, which means that the center density must lie on the $\alpha = 1 - \beta$ line. By computing the density profile from $x = 0$ to $x = -0.5$ or 0.5, we can identify when the domain walls occur at $x_w = -0.5$ or 0.5 lines. If the domain wall position is greater than 0, the overall microtubule overlap shows higher density at the center rather than at the boundaries.

3. High density

The high-density phase occurs when $\alpha > 0.5$ and the left boundary condition cannot be satisfied. The transition density ρ_t separates the center-maximum and center-minimum density profiles, determined by the value of ρ_L when the transition line intercepts the $x_w = 0.5$ line. If $1 - \beta < \rho_t$, density profile has a local maximum at the center; while $1 - \beta > \rho_t$, the motor density profile has a local minimum at the center.

4. Meissner

The Meissner phase occurs when $\alpha > 0.5$ and $1 - \beta < 0.5$. Both boundary conditions cannot be fulfilled, so the density profile is independent of the boundary conditions.

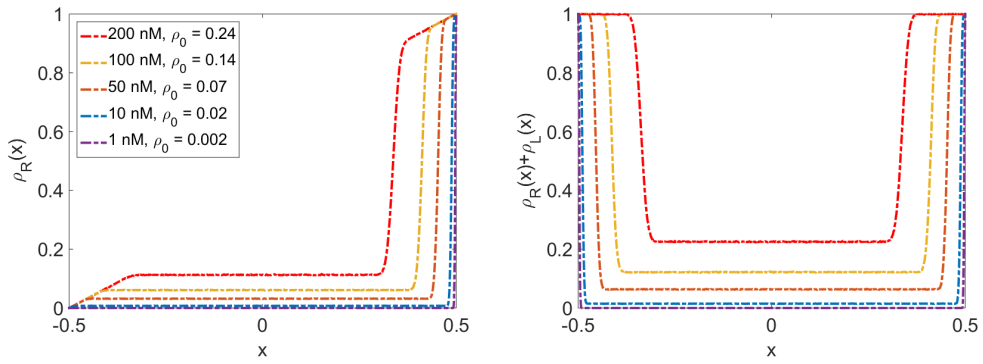

FIG. S6. Motor density profiles for the large-S parameter set. Left: motor density $\rho_R(x)$ on MT with rightward-moving motors. Right: total motor density $\rho_R(x) + \rho_L(x)$ on both MTs in the overlap.

5. *Low density-high density-low density-high density*

The LHLH phase with multiple domain walls occurs when $\alpha < 0.5$ and the switching rate is sufficiently high (fig. 2). The transition points occur where the $C = 0$ analytic solution (equation S18) intersects the transition lines. This makes the flows (fig. S5, blue curve) bounded if the profile is closer to the $\sigma_R = 0$ curve. Thus, the region between the domain wall curves and $\sigma_R = 0$ line is the place where the profiles are bounded which need not only one domain wall but three domain walls in order to connect to the end point.

IV. LARGE SWITCHING RATE PARAMETER SET RESULTS

In fig. S6 we show the motor density profiles for the large-S parameter set.

V. EFFECTS OF THE TOTAL BINDING CONSTRAINT

A. Linear solution near overlap ends

Near the ends of the overlap, the variation of density becomes approximately linear. Consider the left end of the overlap near $x = -1/2$, where $\rho_R \approx 0$ and $\rho_L \approx 1$. This implies that $\sigma_R \approx -1/2$ and $\sigma_L \approx 1/2$, so $\sigma_R \approx -\sigma_L$. Then equations S9 and S10 become approximately

$$\frac{d\sigma_R}{dx} = K_{\text{on}}c + S \tag{S19}$$

$$\frac{d\sigma_L}{dx} = -(K_{\text{off}} + S). \tag{S20}$$

Therefore, near the overlap ends the motor density varies linearly. We can achieve a better approximation to the motor density near the overlap ends by including the density dependence of the

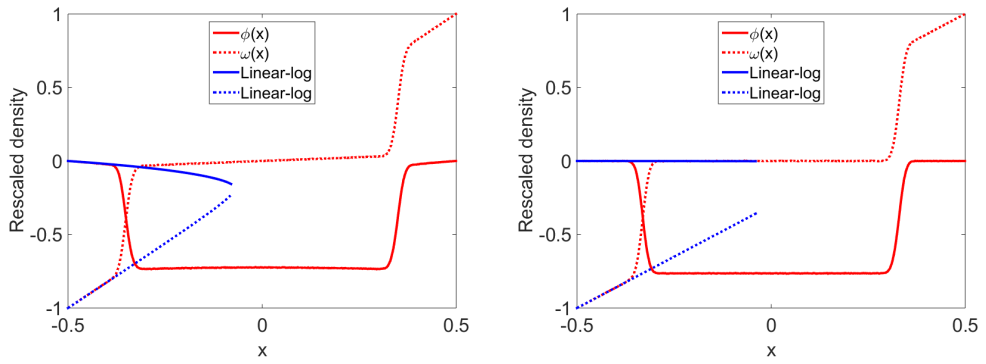

FIG. S7. Comparison of simulation results with approximate solutions valid near overlap ends. Left: experimental parameter set; right: large-S parameter set; both use a bulk motor concentration of 200 nM. Red curves are simulation results, blue curves are approximate solutions valid near the ends of the overlap.

term inversely proportional to density. Then the approximate equations are

$$\frac{d\sigma_R}{dx} = \frac{k+S}{2} - \frac{\gamma}{2\sigma_R} \tag{S21}$$

$$\frac{d\sigma_L}{dx} = -\frac{k+S}{2} + \frac{\gamma}{2\sigma_L}. \tag{S22}$$

An implicit solution for the densities as a function of x is

$$x - x_0 = \frac{2\sigma_R(k+S) + \gamma\log(\gamma - 2(k+S)\sigma_R)}{(k+S)^2} \tag{S23}$$

$$x - x_0 = -\frac{2\sigma_L(k+S) + \gamma\log(\gamma - 2(k+S)\sigma_L)}{(k+S)^2}. \tag{S24}$$

We plot these approximate solutions on the phase plane in fig. S2 and superimposed on the density profiles in fig. S7. As expected, the approximations agree well with simulation results near the overlap ends.

B. Total binding constraint

Motor density profiles must satisfy the total binding constraint of Eqn. 11. We verified that the total binding constraint is satisfied in our simulations by determining the integrated motor density and comparing it to ρ_0 (fig. S8). Whether we vary the bulk motor concentration or the motor speed, we find good agreement between simulations and theory, verifying that Eqn. 11 is satisfied in our model.

To derive an analytic approximation for the motor density, overlap central density, and boundary layer length, we assume the motor densities vary linearly near the filament ends (equations S19 and S20), and that the domain walls are infinitely thin so that we can neglect them in integrating the density. A filament can be divided it into three regions separated by the symmetric boundary

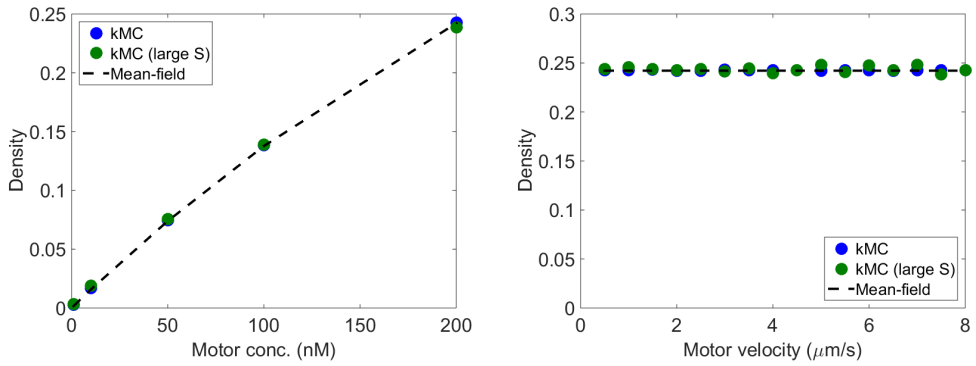

FIG. S8. Total binding constraint. Points show the integral of the motor density on a single filament as described by Eqn. 11. The dashed line is ρ_0. For all simulations performed, the total binding constraint is satisfied.

layer ends are $\pm x_{\rm bl}$ (fig. S9). The density is approximately

$$\rho_R(x) = \begin{cases} (K_{\rm on}c + S)(x + \frac{1}{2}) & -\frac{1}{2} \le x \le -x_{\rm bl} \\ \rho_0 + A\cosh\lambda x + B\sinh\lambda x & -x_{\rm bl} \le x \le x_{\rm bl} \\ (K_{\rm off} + S)(x - \frac{1}{2}) + 1 & x_{\rm bl} \le x \le \frac{1}{2} \end{cases} \tag{S25}$$

The middle formula in equation S25 is the solution of equations 9 and 10 if we neglect the nonlinear terms, which is a good approximation since the the density profile doesn't change much with position in the central region. The constant λ is defined by $\lambda^2 = (K_{\rm on}c + K_{\rm off} + 2S)(K_{\rm on}c + K_{\rm off})$ and ρ_0 is the Langmuir density. The coefficients A and B are derived by using continuity in the density at left end, $(K_{\rm on}c + S)(\frac{1}{2} - x_{\rm bl})$, and continuity in the flux at the right end, $1 - ((K_{\rm off} + S)(x_{\rm bl} - \frac{1}{2}) + 1) = (K_{\rm off} + S)(\frac{1}{2} - x_{\rm bl})$. Then we find

$$A = \frac{(\frac{1}{2} - x_{\rm bl})(K_{\rm on}c + K_{\rm off} + 2S) - 2\rho_0}{2\cosh(\lambda x_{\rm bl})} \tag{S26}$$

$$B = \frac{(\frac{1}{2} - x_{\rm bl})(K_{\rm off} - K_{\rm on}c)}{2\sinh(\lambda x_{\rm bl})} \tag{S27}$$

For the reference parameter set that we study here, the motor speed is large compared to the other rates, making the dimensionless rates small and therefore $\lambda x \ll 1$. We can then approximate $\cosh(\lambda x) \approx 1$ and $\sinh(\lambda x) \approx \lambda x$.

We then find the approximate form of the density profile

$$\rho_R(x) = \begin{cases} (K_{\rm on}c + S)\left(x + \frac{1}{2}\right) & -\frac{1}{2} \le x \le -x_{\rm bl} \\ \frac{x}{2x_{\rm bl}}\left(\frac{1}{2} - x_{\rm bl}\right)(K_{\rm off} - K_{\rm on}c) + \frac{1}{2}\left(\frac{1}{2} - x_{\rm bl}\right)(K_{\rm on}c + K_{\rm off} + 2S) & -x_{\rm bl} \le x \le x_{\rm bl} \\ (K_{\rm off} + S)\left(x - \frac{1}{2}\right) + 1 & x_{\rm bl} \le x \le \frac{1}{2} \end{cases} \tag{S28}$$

Plugging this approximation to the density into the total binding constraint (Eqn. 11), we find

$$-\frac{1}{8}(2x_{\rm bl} - 1)(4 + K_{\rm off}(6x_{\rm bl} - 1) + K_{\rm on}c(2x_{\rm bl} + 1) + 8Sx_{\rm bl}) = \rho_0, \tag{S29}$$

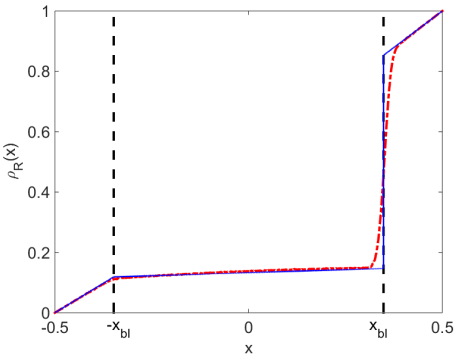

FIG. S9. Motor occupancy and boundary layer ends. Motor density profile $\rho_R(x)$ for rightward-moving motors. Red: kMC simulation results; blue: the linear approximation of Eqn. S28. The ends of the boundary layers are labeled $\pm x_{\rm bl}$. This simulation used the reference parameter set with bulk concentration $c = 200$ nM.

or

$$x_{\rm bl} = \frac{2(S + K_{\rm off} - 1) \pm \sqrt{4(1 - K_{\rm off} - S)^2 + (3K_{\rm off} + K_{\rm on}c + 4S)(4 - 8\rho_0 - K_{\rm off} + K_{\rm on}c)}}{2(3K_{\rm off} + K_{\rm on}c + 4S)}. \quad \text{(S30)}$$

The motor density in the center of the overlap is then

$$\rho_c = \frac{(1 - 2x_{\rm bl})(K_{\rm on}c + K_{\rm off} + 2S)}{4} \quad \text{(S31)}$$

This result shows that the motor density at the center of the overlap is not simply ρ_0, even when the overlap is long. Instead the center density depends on the motor speed and filament switching rate in addition to binding parameters. In fig. S9 we show the comparison of the approximate density profile and positions of the ends of the boundary layers. In fig. S10 we compare the analytic predictions for the boundary layer length to results from simulations.

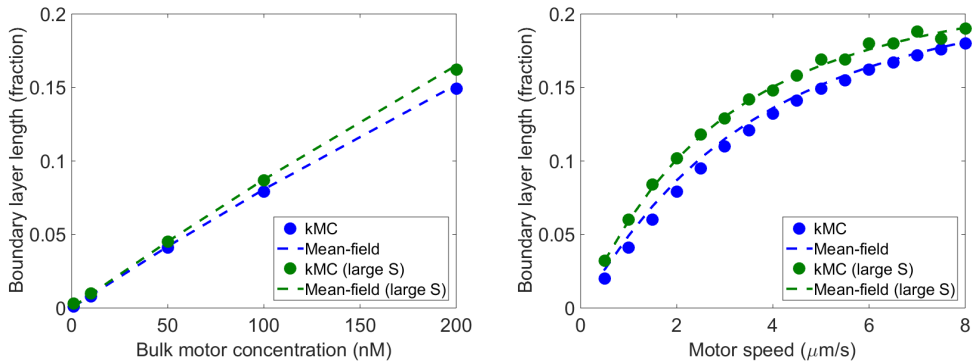

FIG. S10. Length of boundary layer overlap ends where motors accumulate, as a fraction of the total overlap length. Left: variation with bulk motor concentration; right: variation with motor speed. Points indicate simulation results and dashed lines predictions from Eqn. S30.